Estimating intraseasonal intrinsic water-use efficiency from high-resolution tree-ring delta C-13 data in boreal Scots pine forests

Tang, Yu

2023-03

Tang , Y , Sahlstedt , E , Young , G , Schiestl-Aalto , P , Saurer , M , Kolari , P , Jyske , T , Bäck , J & Rinne-Garmston , K T 2023 , ' Estimating intraseasonal intrinsic water-use efficiency from high-resolution tree-ring delta C-13 data in boreal Scots pine forests ' , New Phytologist , vol. 237 , no. 5 , pp. 1606-1619 . https://doi.org/10.1111/nph.18649

http://hdl.handle.net/10138/356233
https://doi.org/10.1111/nph.18649

Research

New Phytologist

Estimating intraseasonal intrinsic water-use efficiency from high-resolution tree-ring $\delta^{13}C$ data in boreal Scots pine forests

Yu Tang[1,2], Elina Sahlstedt[1], Giles Young[1], Pauliina Schiestl-Aalto[3], Matthias Saurer[4], Pasi Kolari[3], Tuula Jyske[5], Jaana Bäck[2] and Katja T. Rinne-Garmston[1]

[1]Bioeconomy and Environment Unit, Natural Resources Institute Finland (Luke), Latokartanonkaari 9, 00790 Helsinki, Finland; [2]Faculty of Agriculture and Forestry, Institute for Atmospheric and Earth System Research (INAR) / Forest Sciences, University of Helsinki, PO Box 27, 00014 Helsinki, Finland; [3]Faculty of Science, Institute for Atmospheric and Earth System Research (INAR) / Physics, University of Helsinki, PO Box 68, 00014 Helsinki, Finland; [4]Forest Dynamics, Swiss Federal Institute for Forest, Snow and Landscape Research (WSL), Zürcherstrasse 111, 8903 Birmensdorf, Switzerland; [5]Production Systems Unit, Natural Resources Institute Finland, Tietotie 2, 02150 Espoo, Finland

Author for correspondence:
Yu Tang
Email: yu.tang@helsinki.fi

Received: *15 June 2022*
Accepted: *16 November 2022*

New Phytologist (2023) **237:** 1606–1619
doi: 10.1111/nph.18649

Key words: eddy covariance, intrinsic water-use efficiency, laser ablation, leaf gas exchange, mesophyll conductance, *Pinus sylvestris* L., postphotosynthetic isotopic fractionation, tree-ring $\delta^{13}C$.

Summary

- Intrinsic water-use efficiency (iWUE), a key index for carbon and water balance, has been widely estimated from tree-ring $\delta^{13}C$ at annual resolution, but rarely at high-resolution intraseasonal scale.
- We estimated high-resolution iWUE from laser-ablation $\delta^{13}C$ analysis of tree-rings ($iWUE_{iso}$) and compared it with iWUE derived from gas exchange ($iWUE_{gas}$) and eddy covariance ($iWUE_{EC}$) data for two *Pinus sylvestris* forests from 2002 to 2019.
- By carefully timing $iWUE_{iso}$ via modeled tree-ring growth, $iWUE_{iso}$ aligned well with $iWUE_{gas}$ and $iWUE_{EC}$ at intraseasonal scale. However, year-to-year patterns of $iWUE_{gas}$, $iWUE_{iso}$, and $iWUE_{EC}$ were different, possibly due to distinct environmental drivers on iWUE across leaf, tree, and ecosystem scales. We quantified the modification of $iWUE_{iso}$ by postphotosynthetic $\delta^{13}C$ enrichment from leaf sucrose to tree rings and by nonexplicit inclusion of mesophyll and photorespiration terms in photosynthetic discrimination model, which resulted in overestimation of $iWUE_{iso}$ by up to 11% and 14%, respectively.
- We thus extended the application of tree-ring $\delta^{13}C$ for iWUE estimates to high-resolution intraseasonal scale. The comparison of $iWUE_{gas}$, $iWUE_{iso}$, and $iWUE_{EC}$ provides important insights into physiological acclimation of trees across leaf, tree, and ecosystem scales under climate change and improves the upscaling of ecological models.

Introduction

How trees respond to climate change has profound impact on the carbon and water balances in forest ecosystems (Mathias & Thomas, 2021). This is because trees regulate stomata to control carbon dioxide uptake during photosynthesis and to control water loss that occurs with transpiration. The trade-off between carbon gain and water loss can be quantified as intrinsic water-use efficiency (iWUE), expressed as the ratio between net assimilation rate and stomatal conductance (Osmond *et al.*, 1980). A common approach to estimate iWUE is via analysis of stable carbon isotope composition ($\delta^{13}C$) of annual tree rings (Farquhar *et al.*, 1982, 1989). However, since tree-ring $\delta^{13}C$ reflects a time-integrated signal (Cernusak, 2020), this method has been rarely applied for detecting high-resolution intraseasonal variations in iWUE (but see Michelot *et al.*, 2011).

Owing to recent advances in online methods for obtaining carbon isotope data from wood, via laser ablation coupled to an isotope ratio mass spectrometry (hereafter LA-IRMS), the ease of determining the intraseasonal tree-ring $\delta^{13}C$ has been greatly improved (Soudant *et al.*, 2016; Rinne-Garmston *et al.*, 2022). A pioneer study, which compared intraseasonal $\delta^{13}C$ data of leaf sucrose and tree rings for *Larix gmelinii* (Rupr.), found similar low-frequency trends for the two records but a systematic isotopic offset, caused by postphotosynthetic isotopic fractionation (Rinne *et al.*, 2015). In future, it needs to be verified that such consistent, common patterns between sucrose and tree-ring $\delta^{13}C$ are also found for other species and site conditions. But considering that $\delta^{13}C$ of leaf sucrose can accurately record iWUE at leaf level (Tang *et al.*, in press) and that the sucrose $\delta^{13}C$ signal is transported to and laid down in tree rings (Gessler *et al.*, 2009), there is high potential to apply LA-IRMS-derived tree-ring $\delta^{13}C$ data for estimating iWUE at intraseasonal scale. As $\delta^{13}C$ signal can be potentially retrieved from tree-ring archives which cover a wide range of areas and periods, such applications, if successful, will be of high value to study the short-term dynamics of CO_2 and H_2O trade, especially for areas and periods without instrumental records.

For a reliable and accurate estimation of iWUE from tree-ring $\delta^{13}C$ (hereafter $iWUE_{iso}$), it is important to quantify how a $\delta^{13}C$ signal may be altered from leaf assimilates to tree rings in postphotosynthetic processes (Fiorella *et al.*, 2022). These processes

include the use of reserves in early growing season (McCarroll *et al.*, 2017; Fonti *et al.*, 2018), isotopic fractionation associated with metabolic processes (Gessler *et al.*, 2009; Rinne *et al.*, 2015), and integration of phloem sugars that are assimilated at different canopy heights (Schleser, 1990; Bögelein *et al.*, 2019). These processes are suggested to be species-specific and site-specific. For example, the use of reserves has been detected for *Quercus petraea* at a temperate forest in Fontainebleau-Barbeau (Vincent-Barbaroux *et al.*, 2019), but not for *Larix gmelinii* Rupr. in the permafrost zone of Central Siberia (Rinne *et al.*, 2015). Furthermore, whereas phloem sugars at breast height originated largely from the upper crown for *Fagus sylvatica*, they originated mainly from the inner and self-shaded crown parts for *Pseudotsuga menziesii* (Bögelein *et al.*, 2019). For a certain site or tree species, concomitant high temporal tracking of leaf sucrose $\delta^{13}C$ along with tree-ring $\delta^{13}C$ measurements can help to quantify the extent of postphotosynthetic $\delta^{13}C$ modification (f_{post}) and the consequent impact on the $iWUE_{iso}$ estimates. Such information can also be used as a guideline in studies conducted under similar growth conditions for the same species.

The accuracy of $iWUE_{iso}$ calculation may also be improved by the use of a complex photosynthetic discrimination model, for instance, via the explicit consideration of mesophyll (Gimeno *et al.*, 2021; Ma *et al.*, 2021) and photorespiratory effects (Keeling *et al.*, 2017; Schubert & Jahren, 2018). Nevertheless, implementing the complex version of photosynthetic discrimination model can be difficult (Lavergne *et al.*, 2019, 2022), partly due to a limited understanding of mesophyll conductance (g_m) and photorespiration dynamics, both of which are dependent on plant species and leaf environment (Sun *et al.*, 2014; Schubert & Jahren, 2018). Hence, the simplified model (Farquhar *et al.*, 1982, 1989) has been applied in the majority of $iWUE_{iso}$ reconstruction studies (e.g. Frank *et al.*, 2015; Guerrieri *et al.*, 2019). However, it is worthwhile to evaluate how mesophyll and photorespiratory effects may impact $iWUE_{iso}$ estimates, as this may help to reconcile the trends and absolute values of iWUE derived from different methods.

Intrinsic water-use efficiency can be also estimated from gas exchange and eddy covariance (EC) measurements ($iWUE_{gas}$ and $iWUE_{EC}$, respectively; e.g. Keenan *et al.*, 2013; Medlyn *et al.*, 2017). $iWUE_{gas}$, $iWUE_{iso}$, and $iWUE_{EC}$ represent signals at different scales: leaf level, whole-tree level, and ecosystem level, respectively. Comparisons between these 'scale-specific' methods not only reveal the limitations of each method (Medlyn *et al.*, 2017) but also show promise to cross-validate different sources of iWUE data (Guerrieri *et al.*, 2019). Since the gas exchange and EC data are of high temporal resolution, they can overall help verify the intraseasonal pattern of iWUE derived from tree-ring $\delta^{13}C$ data, albeit uncertainties exist in each iWUE estimation method (Medlyn *et al.*, 2017; Knauer *et al.*, 2018; Lavergne *et al.*, 2019). The three methods have been scantly compared for their absolute iWUE values, at a global scale for different plant functional types (Medlyn *et al.*, 2017) or at a local site for different tree species (Yi *et al.*, 2019). Studies that compare temporal changes in these iWUE estimates have not been published at intraseasonal scale, and few exist at interannual resolution (Guerrieri *et al.*, 2019; Lavergne *et al.*, 2019). Previous studies have demonstrated a site-specific (Martínez-Sancho *et al.*, 2018; Marchand *et al.*, 2020) and temporally dynamic (Liu *et al.*, 2014; Wieser *et al.*, 2018) response of interannual iWUE to environmental drivers. Further knowledge on the scale-specific temporal trends of iWUE is not only valuable for in-depth understanding of tree physiological responses to environmental change but also can improve the upscaling of ecological models.

The main objective of this study was to evaluate the reliability of high-resolution tree-ring $\delta^{13}C$ data to estimate intraseasonal changes in iWUE. For this purpose, we (1) compared the intraseasonal trends and absolute values of $iWUE_{iso}$, derived from tree-ring LA-IRMS $\delta^{13}C$ analysis, with that of $iWUE_{EC}$ and $iWUE_{gas}$. The comparison was made using a unique set of EC and gas exchange data covering the period from 2002 to 2019, at two Scots pine-dominated boreal forests with contrasting growth conditions. Next, in the effort to reconcile differences between absolute values of the three iWUE series, we (2) quantified the impact of f_{post}, g_m, and photorespiration on $iWUE_{iso}$ estimates. Furthermore, we (3) discussed the environmental and physiological controls on $iWUE_{iso}$, $iWUE_{gas}$, and $iWUE_{EC}$ at both intraseasonal and interannual scales, and strengths and weaknesses of each iWUE estimation method.

Materials and Methods

Site description and environmental data

The study was conducted at two boreal forests dominated by Scots pine (*Pinus sylvestris* L.) in northern and southern Finland (Fig. S1), both of which belong to the Stations for Measuring Ecosystem-Atmosphere Relations (SMEAR) network. The northern site, Värriö, is close to the arctic-alpine timberline for Scots pine. The growth conditions are harsher in Värriö, evident in the lower tree heights, sparser canopy (Fig. S1), lower temperature, and shorter growing season, compared with Hyytiälä (Table S1). More characteristics of the study sites are listed in Table S1.

Air temperature (T) and relative humidity (RH) at the canopy height (16.8 m in Hyytiälä and 9 m in Värriö), precipitation, soil moisture at the topsoil, and air pressure (P_a) at ground level were retrieved from the AVAA Smart SMEAR portal (https://smear.avaa.csc.fi/). Vapor pressure deficit (VPD) was calculated from T and RH. Cumulative precipitation and the means of other environmental variables at half-hourly scale and during the daytime, which was defined as the period from 2 h after sunrise to 2 h before sunset, were calculated.

Sampling and $\delta^{13}C$ analysis

Sampling To determine f_{post} from leaf sugars to phloem sugars and eventually to tree rings, we collected needle and phloem samples during the season 2018 at both sites. One-year-old needles (1 N) and current-year needles (0 N) were collected every 1 or 2 wk from the sun-exposed top canopy of five mature trees for sugar $\delta^{13}C$ analysis. Sampling started before the onset of radial growth (early May in Hyytiälä and late May in Värriö) and ended

after the cessation of radial growth (October in both sites), conducted all together 20 times per site. Phloem samples were collected at breast height from five mature trees on 6 d per site and season, twice in May and once per month from June to September. Needle and phloem samples were put in a cool box immediately upon collection, and microwaved at 600 W for 1 min within 2 h to stop metabolic activities (Wanek *et al.*, 2001). Tree-ring samples were taken at breast height after the cessation of growth in 2019. In Värriö, one 5-mm-diameter core sample was collected from five mature trees, while in Hyytiälä, five trees were felled, and cross sections were obtained. Average $\delta^{13}C$ from five trees was used to represent the average conditions experienced by trees at the study sites (Leavitt & Long, 1984). All sampled trees were within the 80% footprint boundaries of the EC towers, which are *c.* 400 m in Hyytiälä (Launiainen *et al.*, 2022) and 200 m in Värriö (Kulmala *et al.*, 2019).

$\delta^{13}C$ of leaf and phloem sugars Water-soluble carbohydrates (WSCs) were extracted and purified from homogenized needle and phloem samples, according to Wanek *et al.* (2001) and Rinne *et al.* (2012). Briefly, the supernatant was separated from the water extraction at 85°C and then purified by three types of sample preparation cartridges (Dionex OnGuard II H, A and P; Thermo Fisher Scientific, Waltham, MA, USA). The purified WSCs were lyophilized, dissolved in deionized water, and filtered through a 0.45-μm syringe filter (Acrodisc).

$\delta^{13}C$ of WSCs was measured using an elemental analyzer (EA; Europa EA-GSL; Sercon Ltd, Crewe, UK) coupled to an IRMS (20–22 IRMS; Sercon Ltd) at the Stable Isotope Laboratory of Luke (SILL) at Natural Resources Institute Finland (Luke, Helsinki). Before $\delta^{13}C$ analysis, aliquots of solubilized WSCs were pipetted into individual tin capsules (IVA Analysentechnik, Meerbusch, Germany), freeze-dried, and wrapped. Three reference materials were used to calibrate the $\delta^{13}C$ values of WSCs, IAEA-CH3 (cellulose, −24.724‰), IAEA-CH7 (polyethylene, −32.151‰), and an in-house sucrose reference (Sigma-Aldrich, −12.22‰). Repeat measurement of a quality control material indicates a measurement precision of 0.1‰ (SD). $\delta^{13}C$ of leaf WSCs was calculated as the average $\delta^{13}C$ of WSCs in 1 N and 0 N.

$\delta^{13}C$ values of sucrose were analyzed at WSL (Birmensdorf, Switzerland), using a Delta V Advantage IRMS (Thermo Fisher Scientific) coupled with a high-performance liquid chromatography (HPLC) system with a Finnigan LC Isolink interface (Thermo Fisher Scientific) (Rinne *et al.*, 2012). External sucrose standards, with known $\delta^{13}C$ values and comparable concentrations to samples (from 20 to 180 ng C μl^{-1}), were analyzed every 10 samples. Correction for HPLC-IRMS $\delta^{13}C$ values was performed according to Rinne *et al.* (2012). The measurement precision of sucrose standards was 0.26‰ (SD). $\delta^{13}C$ of leaf sucrose was calculated as the average $\delta^{13}C$ of sucrose in 1 N and 0 N.

$\delta^{13}C$ of tree rings Tree-ring samples were air-dried before the preparation for isotope analysis. Each sample was sanded with progressively finer grades of sandpaper until ring boundaries and individual cells were clearly identifiable. To ensure that any sawdust collected in voids and intercellular spaces did not affect the isotope signal, each sample was placed in distilled water in an ultrasonic bath for 30 min to remove the sawdust. Samples were then visually inspected under a binocular microscope. Tree rings were measured using WinDendro™ and statistically cross-matched against local chronologies to ensure the correct year was assigned to each ring. Mobile resin and extractives of the samples were removed using a 2 : 1 mixture of toluene and ethanol in a Soxhlet extractor for a duration of 48 h (Loader *et al.*, 1997). After extraction, any residual toluene and ethanol in the samples were removed by rinsing the samples with distilled water in the Soxhlet extractor. Samples were then air-dried. Resin-extracted wood was used for LA-IRMS analysis, as suggested by Schulze *et al.* (2004).

Intraseasonal $\delta^{13}C$ was analyzed for each tree-ring sample using LA-IRMS at SILL (Methods S1), following the operation principle by Schulze *et al.* (2004) and Loader *et al.* (2017). In brief, ablated dust particles were carried by helium flow through a combustion device, the resulting CO_2 was collected with liquid nitrogen, and subsequently, the CO_2 was released upon heating and purified in a GC-column before its introduction to IRMS. A series of 40 μm tangential laser tracks were sampled along the same radial direction on tree rings at an interval of 40 μm (years from 2010 to 2019) or 80 μm (Fig. 1a). Depending on the ring width, between 5 and 33 laser tracks per tree ring were ablated for $\delta^{13}C$ analysis. Each sample was run against an in-house CO_2 reference gas. The raw $\delta^{13}C$ values were calibrated against USGS-55 (Mexican ziricote tree powder, −27.13‰) and an in-house reference (yucca plant powder, −15.46‰), which were both measured concurrently with the tree-ring samples. The USGS-55 and the in-house reference were in the form of a 10-mm-diameter disk, which had been prepared by compressing powder using a manual hydraulic press, providing a smooth, solid surface for ablation. In addition, IAEA-C3 cellulose paper was measured multiple times during each run for quality control of the produced $\delta^{13}C$ values. The LA-IRMS measured $\delta^{13}C$ value for IAEA-C3 was −24.69 ± 0.24‰, which is in line with the certified value of −24.91 ± 0.49‰. Spot sizes and track lengths of the reference materials were varied to produce variation in signal size, which enabled monitoring of a size effect on $\delta^{13}C$ values, and the data were corrected when needed (Werner & Brand, 2001).

Averaging and timing intraseasonal $\delta^{13}C$

Individual tree-ring $\delta^{13}C$ series had in general similar intraseasonal patterns (Figs S2, S3), enabling the calculation of site-representative tree-ring $\delta^{13}C$ series. First, considering tree-to-tree differences in tree-ring widths, we aligned the intraseasonal tree-ring $\delta^{13}C$ data against their relative position within a tree ring (from 0 to 1) per tree, year, and site. Then, we interpolated tree-ring $\delta^{13}C$ per tree, year, and site against relative position from 0.05 to 1 at an interval of 0.05 (Figs S2, S3). Finally, we calculated site-representative tree-ring $\delta^{13}C$ as averages of five tree rings at the interpolated relative position.

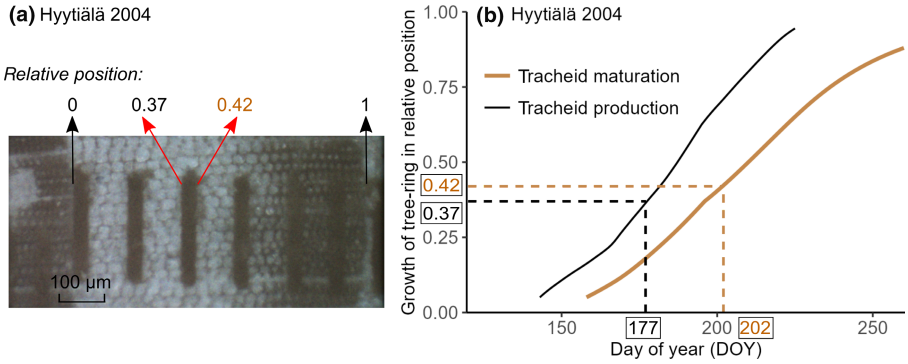

Fig. 1 Example of how the formation period of a tree-ring $\delta^{13}C$ measurement of Scots pine was defined. (a) Relative position of a tree-ring $\delta^{13}C$ measurement within a tree ring; (b) formation period of the tree-ring $\delta^{13}C$ measurement based on the growth curves of tracheid production and tracheid maturation for the specific year and site. The growth curves were modeled via the Carbon Allocation Sink Source Interaction model (Schiestl-Aalto *et al.*, 2015). First, the relative position of a $\delta^{13}C$ measurement within a tree ring was defined, for example from 0.37 to 0.42 in (a). Then, the initial development date of the tracheids representing that $\delta^{13}C$ measurement was determined, according to the tracheid production curve in (b) (day of year, DOY) 177 for relative position 0.37). Next, the date was defined when the tracheids for that $\delta^{13}C$ measurement were fully mature, according to the tracheid maturation curve (DOY 202 for relative position 0.42). Finally, the obtained period representing a tree-ring $\delta^{13}C$ value and intrinsic water-use efficiency derived therefrom ($iWUE_{iso}$), in this case from DOY 177 to DOY 202, was used to align $iWUE_{iso}$ with iWUE derived from eddy covariance ($iWUE_{EC}$) and gas exchange ($iWUE_{gas}$) data.

To time intraseasonal tree-ring $\delta^{13}C$, tree-ring growth curves against day of year (DOY) were simulated per year and site via a dynamic growth model *Carbon Allocation Sink Source Interaction* (CASSIA; Schiestl-Aalto *et al.*, 2015). The performance of CASSIA model results was evaluated by comparison with xylogenesis observational results for years 2007, 2008, 2009, 2018, and 2019, for both sites (Methods S2; Fig. S4). With simulated growth curves, the start DOY of tracheid production and the end DOY of tracheid maturation could be determined for each site-representative tree-ring $\delta^{13}C$ data point (Fig. 1).

iWUE estimates

iWUE from leaf gas exchange ($iWUE_{gas}$) CO_2 fluxes (A) and H_2O fluxes (E) were measured online with leaf gas exchange systems, as described by Altimir *et al.* (2002) and Aalto *et al.* (2014) from 2002 to 2019 at both sites. However, no data were available for years 2005 and 2014 in Hyytiälä. In brief, transparent acrylic plastic chambers were installed at the top canopy of one to four mature trees with a debudded 1- or 2-yr-old shoot enclosed. Four chamber designs were employed over the years in Hyytiälä, whereas the chamber design in Värriö was the same all the time. The non-airtight chambers were automatically closed intermittently for 50 to 80 times (in Hyytiälä) or 150 to 180 times (in Värriö) per day, with sample air drawn to gas analyzers (URAS-4; Hartmann & Braun, Siek, Germany; LI-840; Li-Cor, Lincoln, NE, USA). CO_2 fluxes and E were calculated from instantaneous CO_2 and H_2O records taken during the first 30–40 s of chamber closure (Kolari *et al.*, 2012). Flux data were omitted when RH exceeded 85% to avoid biased results due to adsorption of water on chamber walls and tubing (Altimir *et al.*, 2006). Small fluxes ($A < 0.5$ µmol m^{-2} s^{-1} and $E < 0.1$ mmol m^{-2} s^{-1}) were also discarded given the uncertainties they may cause in the calculation of $iWUE_{gas}$. Half-hourly A and E data series were produced and applied to calculate $iWUE_{gas}$ (Eqn 1; Beer *et al.*, 2009), where g is stomatal conductance. In the well-stirred chambers, boundary layer conductance is high (Uddling & Wallin, 2012) and thus for simplicity not considered in the calculation of $iWUE_{gas}$.

$$iWUE_{gas} = A/g = A/E \cdot (VPD/P_a) \quad \text{Eqn 1}$$

iWUE from eddy covariance ($iWUE_{EC}$) The net ecosystem CO_2 exchange (NEE) and H_2O flux (ET) were measured using a closed-path EC system above the stand at 24 m height from 2002 to 2017 and at 27 m height from 2018 to 2019 in Hyytiälä, and at 16.6 m height from 2012 to 2019 in Värriö. Briefly, the EC data were: screened for outliers and erroneous measurements using standard methods (Aubinet *et al.*, 2012); filtered by the turbulence criteria (Markkanen *et al.*, 2001); averaged to half-hourly scale and gap-filled (Kulmala *et al.*, 2019); and corrected for the storage of CO_2 below the measuring height (Kolari *et al.*, 2009; Launiainen *et al.*, 2016). Half-hourly gross primary production (GPP) was calculated by subtracting the modeled total ecosystem respiration from NEE (Kulmala *et al.*, 2019). Furthermore, half-hourly GPP and ET data were discarded, when precipitation occurred before the measurements, or when RH was higher than 85% to minimize the effect of condensation on canopy surfaces or instruments. More detailed description of the EC systems can be found in Vesala *et al.* (2005) and Kulmala *et al.* (2019), and EC data processing in Launiainen *et al.* (2016) and Mammarella *et al.* (2016). Assuming infinite aerodynamic conductance and no contribution of nontranspiratory water fluxes, half-hourly $iWUE_{EC}$ was calculated from GPP and ET data by Eqn 2 (Beer *et al.*, 2009), where G_s is surface conductance. Twenty-three percentage of half-hourly EC data were gap-filled. Using the gap-filled data had limited impact on the temporal trends and absolute values of $iWUE_{EC}$, considering that the $iWUE_{EC}$ series with and without days that had high percentage (≥ 50%) of gap-filled flux records were highly correlated ($r = 0.98$, $P < 0.001$).

$$iWUE_{EC} = GPP/G_s = GPP/ET \cdot (VPD/P_a) \quad \text{Eqn 2}$$

iWUE from tree-ring $\delta^{13}C$ ($iWUE_{iso}$) Intrinsic water-use efficiency can also be estimated from isotope data via the photosynthetic discrimination model of Farquhar *et al.* (1982, 1989) (Eqns 3–6).

$$iWUE_{iso} = (c_a - c_i)/1.6 \quad \text{Eqn 3}$$

$$\Delta = a + (b-a) \cdot \frac{c_i}{c_a} - (b-a_m) \cdot A/(g_m \cdot c_a) - f \cdot \Gamma_*/c_a \quad \text{Eqn 4}$$

$$\Gamma_* = 42.75 \cdot \exp[37830 \cdot (T_k - 298)/(298 \cdot R \cdot T_k)] \quad \text{Eqn 5}$$

$$\Delta = (\delta^{13}C_{air} - \delta^{13}C_{tree})/(1 + \delta^{13}C_{tree}/1000) \quad \text{Eqn 6}$$

c_a and c_i are the atmospheric and intercellular CO_2 concentrations, respectively; Δ is the photosynthetic discrimination; a (4.4‰) is the fractionation due to diffusion of CO_2 through stomata; b (29‰) is the fractionation due to carboxylation; a_m (1.8‰) is the fractionation during the mesophyll CO_2 transfer; f is the fractionation during photorespiration; Γ_* is the CO_2 compensation point in the absence of dark respiration in μmol mol^{-1}, estimated according to Eqn 5 (Bernacchi *et al.*, 2001); T_k is the leaf temperature in K, taken as the air T measured inside the chamber; R is the universal gas constant (8.3145 J mol^{-1} K^{-1}); $\delta^{13}C_{air}$ is the $\delta^{13}C$ of atmospheric CO_2; and $\delta^{13}C_{tree}$ is the site-representative $\delta^{13}C$ of the tree rings (resin-extracted whole wood). Event-based c_a and $\delta^{13}C_{air}$ values in a northern Finnish site, Pallas (67°58′N, 24°7′E, 565 m asl (above sea level), https://gml.noaa.gov/dv/site/PAL.html), the closest site with continuous records for both c_a and $\delta^{13}C_{air}$, were interpolated to daily scale and used. As there were no $\delta^{13}C_{air}$ data observed during 2015 to 2019 in Pallas, we estimated $\delta^{13}C_{air}$ from c_a and the linear regression between $\delta^{13}C_{air}$ and c_a in Pallas (Fig. S5). The average c_a and $\delta^{13}C_{air}$ for the formation period of each tree-ring $\delta^{13}C$ measurement were used as the input for Eqns 3, 4, 6. Fractionation associated with day respiration was not considered here, considering that day respiration is intensively inhibited (Keenan *et al.*, 2019) and has insignificant impact on Δ when net assimilation rate is high (Busch *et al.*, 2020).

To test the impact of mesophyll and photorespiratory terms on $iWUE_{iso}$, we took following assumptions: with no explicit consideration of g_m and f, by setting $g_m = \infty$, $f = 0$, and $b = 27‰$, which is the simplified model widely used for estimating $iWUE_{iso}$; constant g_m of 0.127 mol m^{-2} s^{-1}, corrected for all-sided leaf area (Stangl *et al.*, 2019) and $f = 8‰$ (Ghashghaie *et al.*, 2003); constant g_m and $f = 16‰$ (Evans & von Caemmerer, 2013); dynamic g_m varying with T (Methods S3; Sun *et al.*, 2014) and $f = 8‰$; dynamic g_m and $f = 16‰$. We compared how the absolute values of $iWUE_{iso}$ changed across different assumptions, and evaluated whether the intraseasonal variations or interannual trends of $iWUE_{iso}$ varied between different assumptions. In later sections, $iWUE_{iso}$ from the simplified model was reported, unless otherwise specified.

Data analysis

To align $iWUE_{gas}$, $iWUE_{EC}$, and $iWUE_{iso}$ at intraseasonal scale, we averaged daytime $iWUE_{gas}$ and $iWUE_{EC}$ over the period representing each $iWUE_{iso}$ estimate (Fig. 1). For simplicity, we did not consider changes in carbon allocation rate over time. Phloem transport time from top canopy to breast height was set to 2 d in Hyytiälä and 1 d in Värriö, according to Mencuccini & Hölttä (2010), that is, each period representing an $iWUE_{iso}$ estimate (Fig. 1) was corrected for these lags. Due to differences in absolute values of iWUE and a more dampened trend in $iWUE_{iso}$ in comparison with the other records, iWUE series were z-scored per site, year, and method for intraseasonal comparisons. Pearson correlations between the three iWUE series were calculated per year and site.

For annual values of iWUE, we compared the means of each iWUE series for the growing periods of earlywood, latewood, and the whole tree ring. To examine the significance of interannual iWUE trends, we applied the Mann–Kendall trend test with R package 'Kendall' (McLeod, 2011). All statistical analyses were made in R v.4.0.0 (R Core Team, 2020).

Results

Comparison of intraseasonal patterns of iWUE

In Hyytiälä, $iWUE_{iso}$ aligned in the intraseasonal trends with $iWUE_{EC}$ and/or $iWUE_{gas}$, except for year 2019 (Fig. 2), the year that had the smallest variations in T between June, July, and August (15.7°C, 15.9°C, and 15.2°C, respectively) among the studied years and had a small variability in tree-ring $\delta^{13}C$ (−27.0 ± 0.2‰). $iWUE_{iso}$ aligned clearly better with $iWUE_{gas}$ than with $iWUE_{EC}$ in years 2006, 2007, 2009, 2010, 2011, and 2016, which were marked by significantly higher VPD in June compared with other years (0.74 kPa vs 0.56 kPa, $P = 0.002$). In comparison, $iWUE_{iso}$ aligned better with $iWUE_{EC}$ than with $iWUE_{gas}$ in years 2003, 2004, 2013, and 2018. These years had higher soil temperature in May than the other years (6.9°C vs 5.8°C), although the difference was not significant ($P = 0.08$).

In Värriö, $iWUE_{iso}$, $iWUE_{EC}$, and $iWUE_{gas}$ aligned with each other in the intraseasonal trends except for year 2012 (Fig. 3). In this year, albeit showing a similar low-frequency trend, $iWUE_{EC}$ and $iWUE_{iso}$ were not significantly correlated. In year 2012, the site experienced a dry period, with lowest precipitation amount in August among the studied years.

For both sites, the intraseasonal trends of $iWUE_{iso}$ were clearly more dampened than that of $iWUE_{EC}$ and $iWUE_{gas}$, when absolute values instead of z-scores were compared. The amplitudes of intraseasonal variations in $iWUE_{iso}$, $iWUE_{gas}$, and $iWUE_{EC}$ were 13 ± 6, 24 ± 8, and 29 ± 9 ppm, respectively, in Hyytiälä, and 8 ± 3, 19 ± 6, and 30 ± 14 ppm, respectively, in Värriö. This dampened intraseasonal variation in $iWUE_{iso}$ corresponded to a lower amplitude of intraseasonal variability in tree-ring $\delta^{13}C$ compared with leaf sucrose $\delta^{13}C$ (1.3‰ vs 4.3‰ in Hyytiälä; 1.3‰ vs 4.2‰ in Värriö; Fig. S6).

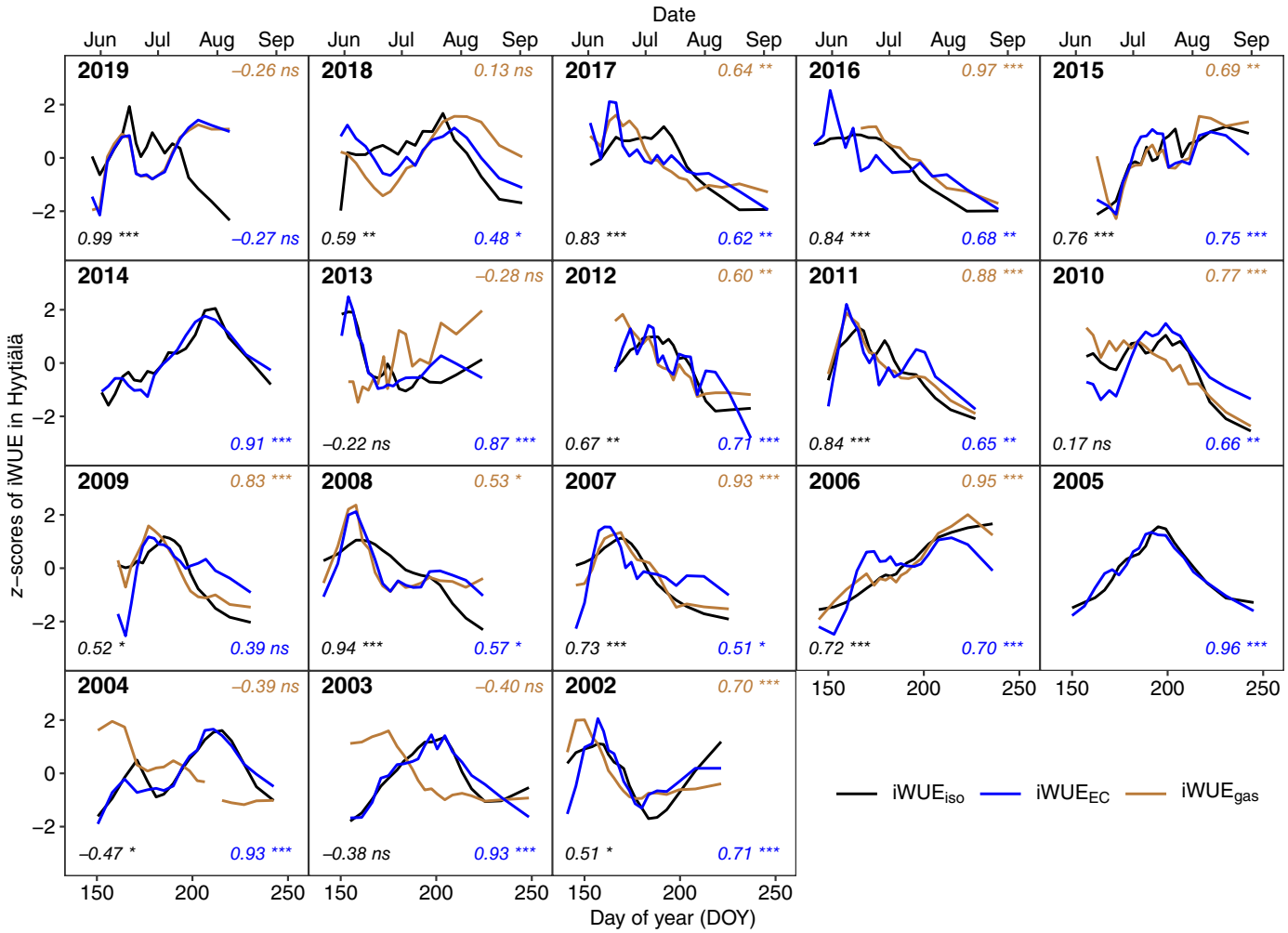

Fig. 2 *Z*-scores of intrinsic water-use efficiency (iWUE) of Scots pine from 2002 to 2019 in Hyytiälä. Intrinsic water-use efficiency was derived from gas exchange ($iWUE_{gas}$), tree-ring $\delta^{13}C$ ($iWUE_{iso}$), and eddy covariance ($iWUE_{EC}$) data. For each year, the Pearson correlation coefficient and significance level for $iWUE_{gas}$ and $iWUE_{iso}$ (upper right), $iWUE_{EC}$ and $iWUE_{iso}$ (lower right), and $iWUE_{gas}$ and $iWUE_{EC}$ (lower left) are given: *, $P < 0.05$; **, $P < 0.01$; ***, $P < 0.001$; ns, not significant. Middle day of year (DOY) of the formation period representing each $iWUE_{iso}$ data point is presented.

Comparison of interannual patterns of iWUE

For each three iWUE estimates, the average absolute value of iWUE did not significantly differ between the growing periods of earlywood, latewood, and the whole ring ($P > 0.05$, Fig. S7). Hence, for examining interannual iWUE variability, we used the average iWUE values for the whole growing season. Annual $iWUE_{gas}$ presented a statistically significant increasing trend in both Värriö (1.4 ppm yr^{-1}, $P = 0.01$) and Hyytiälä (1.5 ppm yr^{-1}, $P = 0.03$; Fig. 4). Annual $iWUE_{iso}$ and $iWUE_{EC}$ did not significantly increase during the studied period in Värriö (0.8 ppm yr^{-1}, $P = 0.20$ and 0.9 ppm yr^{-1}, $P = 0.54$, respectively) or Hyytiälä (0.7 ppm yr^{-1}, $P = 0.06$ and −0.2 ppm yr^{-1}, $P = 0.40$, respectively; Fig. 4). Annual $iWUE_{gas}$, $iWUE_{iso}$, and $iWUE_{EC}$ were not significantly correlated with each other for either site (Fig. 4). Among all tested environmental variables, which were c_a, RH, T, VPD and soil moisture, annual $iWUE_{gas}$ correlated best with c_a at both sites (Table 1), whereas annual $iWUE_{iso}$ and $iWUE_{EC}$ correlated best with VPD (Table 1).

Impact of f_{post}, g_m, and f on $iWUE_{iso}$

To reconcile differences between $iWUE_{iso}$, $iWUE_{gas}$, and $iWUE_{gas}$, we evaluated the impact of f_{post}, g_m, and f on $iWUE_{iso}$.

f_{post} differed between the two sites, thus posing site-specific impacts on $iWUE_{iso}$. Among all analyzed carbon pools, leaf WSCs had the lowest $\delta^{13}C$ values, whereas phloem sucrose had the highest $\delta^{13}C$ values (Fig. 5). Water-soluble carbohydrates were significantly ^{13}C-depleted in comparison with sucrose in both leaves ($P < 0.001$ for both sites) and phloem ($P < 0.001$ for both sites) (Fig. 5), due to the contribution of pinitol/*myo*-inositol (33 ± 6% in leaves, and 18 ± 4% in phloem) with low $\delta^{13}C$ values (−31.4 ± 0.4‰ in leaves, −30.6 ± 0.6‰ in phloem). In Hyytiälä, tree-ring $\delta^{13}C$ was 0.9‰ ($P < 0.001$), 2.8‰ ($P < 0.001$), and 0.7‰ ($P = 0.03$) higher than $\delta^{13}C$ of leaf sucrose, leaf WSCs, and phloem WSCs, respectively, but 0.4‰ ($P = 0.24$) lower than $\delta^{13}C$ of phloem sucrose (Fig. 5a). In Värriö, the $\delta^{13}C$ differences from tree rings to leaf sucrose, leaf WSCs, phloem WSCs, and phloem sucrose were 0‰

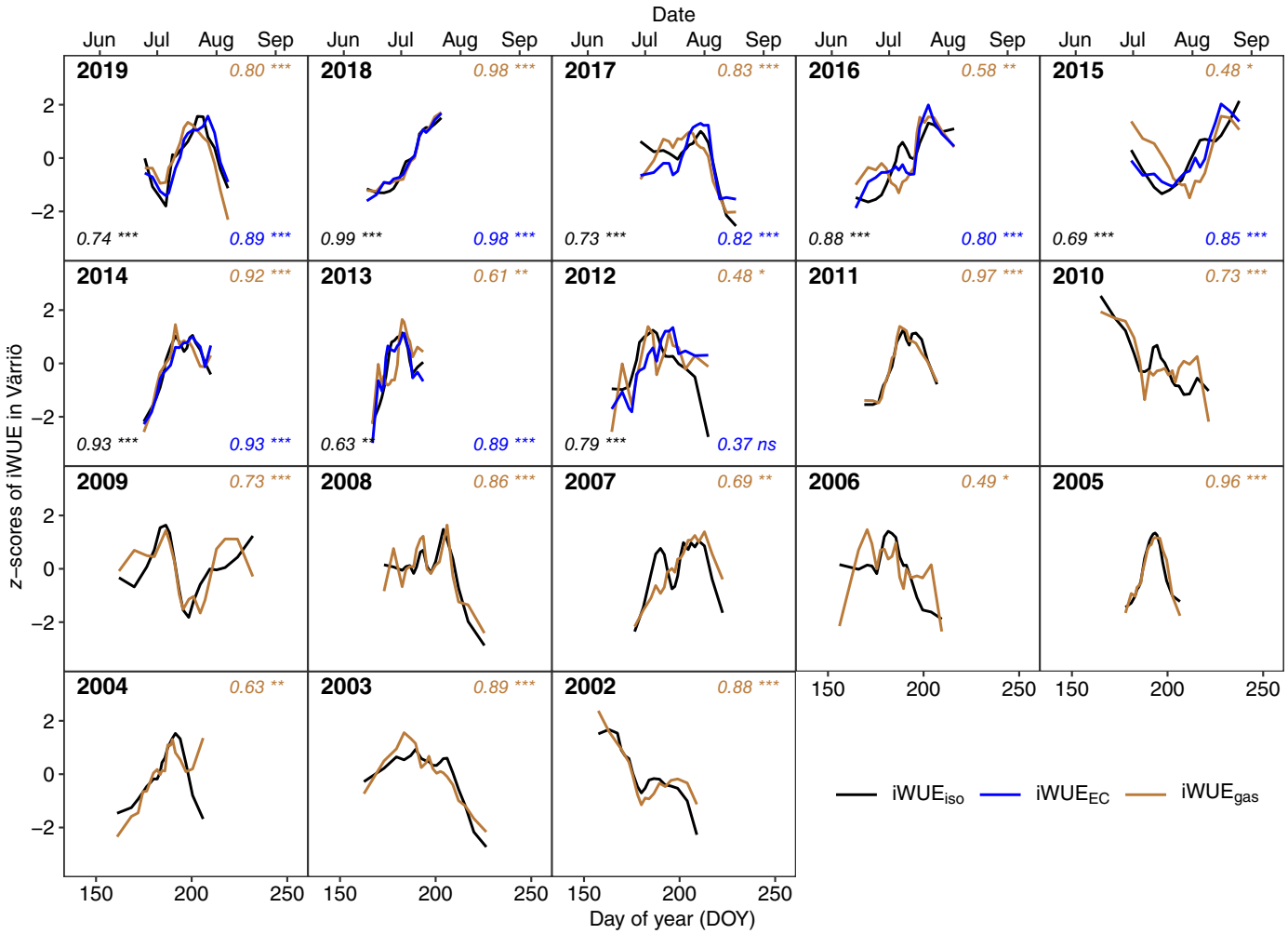

Fig. 3 *Z*-scores of intrinsic water-use efficiency (iWUE) of Scots pine from 2002 to 2019 in Värriö. Intrinsic water-use efficiency was derived from gas exchange ($iWUE_{gas}$), tree-ring $\delta^{13}C$ ($iWUE_{iso}$), and eddy covariance ($iWUE_{EC}$) data. For each year, the Pearson correlation coefficient and significance level for $iWUE_{gas}$ and $iWUE_{iso}$ (upper right), $iWUE_{EC}$ and $iWUE_{iso}$ (lower right), and $iWUE_{gas}$ and $iWUE_{EC}$ (lower left) are given: *, $P < 0.05$; **, $P < 0.01$; ***, $P < 0.001$; ns, not significant. Middle day of year (DOY) of the formation period representing each $iWUE_{iso}$ data point is presented.

($P = 0.99$), 1.6‰ ($P < 0.001$), 0.5‰ ($P = 0.10$), and − 0.7‰ ($P = 0.08$), respectively (Fig. 5b). Common seasonal courses existed in $\delta^{13}C$ variability of leaf sucrose and tree rings for both sites (Fig. S6). In Hyytiälä, both leaf sucrose $\delta^{13}C$ and tree-ring $\delta^{13}C$ presented an inverse 'V' shape variation from June to September (Fig. S6a). In Värriö, $\delta^{13}C$ of tree ring followed the general increasing trend in leaf sucrose for the whole ring formation period (Fig. S6b). Taken together, f_{post} from leaf sucrose to tree rings was 0.9‰ in Hyytiälä but 0.0‰ in Värriö (Fig. 5). By subtracting the 0.9‰ offset from tree-ring $\delta^{13}C$ for Hyytiälä, $iWUE_{iso}$ decreased by 11% (Fig. 6a).

The explicit consideration of g_m and f in the calculation of $iWUE_{iso}$ did not change the intraseasonal or interannual patterns of $iWUE_{iso}$ (Fig. S8), but it lowered the absolute values of $iWUE_{iso}$ for both sites ($P < 0.001$, Fig. 6). Constant g_m ($r = 0.96$, $P < 0.001$) and dynamic g_m ($r = 0.97$, $P < 0.001$) assumptions both produced $iWUE_{iso}$ that linearly correlated with $iWUE_{iso}$ from the simplified model. Similarly, $iWUE_{iso}$ from the assumptions $f = 8‰$ ($r = 0.93$, $P < 0.001$) and $f = 16‰$ ($r = 0.92$, $P < 0.001$) both linearly correlated with $iWUE_{iso}$ from the simplified model.

$iWUE_{gas}$, $iWUE_{iso}$, and $iWUE_{EC}$ differed significantly in their absolute values for both sites ($P < 0.05$), in the following order: $iWUE_{iso} > iWUE_{gas} > iWUE_{EC}$ (Fig. 6). In Hyytiälä, $iWUE_{gas}$ and $iWUE_{EC}$ were on average 19% and 39%, respectively, lower than $iWUE_{iso}$, whereas in Värriö, the differences were 7% and 41%. If applying constant g_m and $f = 8‰$ and correcting $iWUE_{iso}$ by f_{post}, the differences from $iWUE_{iso}$ to $iWUE_{gas}$ and $iWUE_{EC}$ decreased to 1% and 25%, respectively, in Hyytiälä; and to 3% and 39%, respectively, in Värriö (Fig. 6).

Discussion

Validity of tree-ring $\delta^{13}C$ for intraseasonal iWUE estimates

We observed a general agreement in the intraseasonal trends of $iWUE_{iso}$, $iWUE_{gas}$, and $iWUE_{EC}$ (Figs 2, 3), which clearly supports the validity of using tree-ring $\delta^{13}C$ for estimating iWUE at

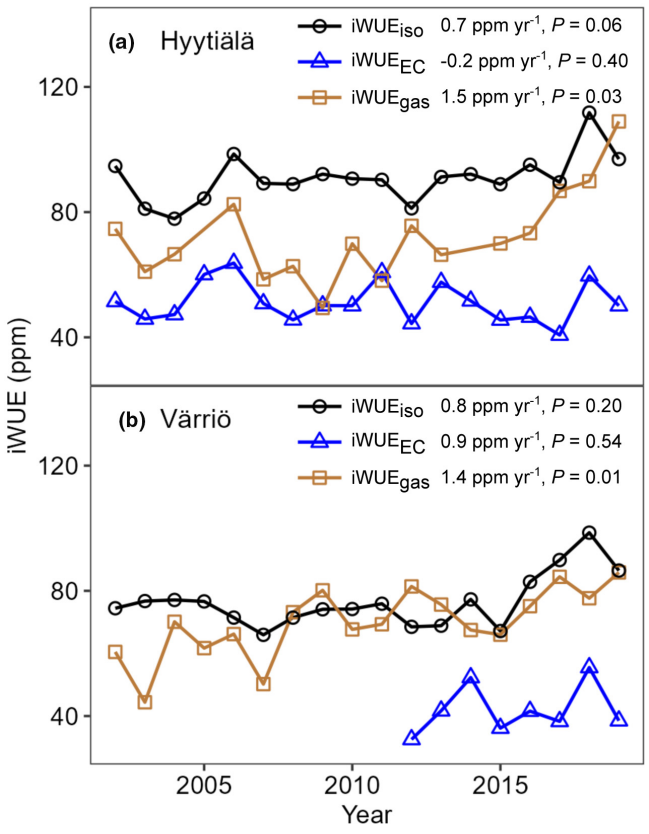

Fig. 4 Interannual intrinsic water-use efficiency (iWUE) of Scots pine derived from gas exchange (iWUE$_{gas}$), eddy covariance (iWUE$_{EC}$), and tree-ring $\delta^{13}C$ (iWUE$_{iso}$) in (a) Hyytiälä and (b) Värriö from 2002 to 2019. Yearly increase rates of iWUE and P values of Mann–Kendall trend test are given. Pearson correlations between iWUE$_{iso}$ and iWUE$_{EC}$, between iWUE$_{gas}$ and iWUE$_{EC}$, and between iWUE$_{iso}$ and iWUE$_{gas}$ were 0.46 (P = 0.05), 0.48 (P = 0.06) and 0.05 (P = 0.87), respectively, in Hyytiälä; and 0.55 (P = 0.16), 0.42 (P = 0.08), and −0.31 (P = 0.46), respectively, in Värriö.

high-resolution intraseasonal scale. This is partly in line with Michelot *et al.* (2011), where the latewood section of deciduous *Quercus petraea* recorded well-seasonal variations in iWUE. Nevertheless, our results indicate that earlywood of boreal conifers can also be a good recorder for iWUE$_{iso}$. This is in line with Kress *et al.* (2010), although earlywood has been removed by default in some earlier annual iWUE$_{iso}$ studies (Waterhouse *et al.*, 2004) in case of possible use of reserves for earlywood growth (McCarroll & Loader, 2004). Our conclusion on the suitability of both earlywood and latewood sections for iWUE$_{iso}$ studies is based on the following observations: variations of iWUE$_{iso}$ during the earlywood growing period aligned with that of iWUE$_{EC}$ and/or iWUE$_{gas}$ (Figs 2, 3); iWUE$_{iso}$ values averaged for the growing periods of earlywood, latewood, and the whole ring were not significantly different (Fig. S7); we did not observe a previous-year reserve $\delta^{13}C$ signal in earlywood (Fig. S9).

Factors affecting iWUE$_{iso}$ estimates

The impact of f_{post}, that is, overall apparent isotope fractionation between tree rings and new assimilates, on iWUE$_{iso}$ has been addressed in earlier studies with a correction factor that has been obtained by measuring $\delta^{13}C$ difference between tree rings and leaf water-soluble organic matter (Frank *et al.*, 2015) or total organic matter (Belmecheri & Lavergne, 2020). Considering that leaf bulk materials have varying and significant $\delta^{13}C$ offsets from new assimilates and that sucrose accurately records assimilate $\delta^{13}C$ (Tang *et al.*, in press), our comparison between tree rings and leaf sucrose presents a more precise quantification of f_{post}. From this comparison, we defined f_{post} of 0.9‰ for Hyytiälä but 0.0‰ for Värriö (Fig. 5), which can reduce iWUE$_{iso}$ by 11% in Hyytiälä (Fig. 6).

In our study, the site-specific f_{post} values were not associated with site-specificity in the use of previous-year reserves for tree-ring growth (Fig. S9) but may be related to site-to-site differences in postphotosynthetic metabolisms. First, f_{post} can be partly ascribed to the remobilization of ^{13}C-enriched transitory starch during the night (Gessler & Ferrio, 2022), which causes an overall ^{13}C-enrichment in phloem sucrose relative to leaf sucrose (Fig. 5). The proportion of starch-derived ^{13}C-enriched sucrose in breast-height phloem depends on the phloem transport velocity and tree height (Gessler & Ferrio, 2022), which differed between Hyytiälä and Värriö (Table S1). Second, f_{post} can be affected by the mixing of assimilates formed at different canopy heights, which may have a $\delta^{13}C$ gradient of up to 8‰ (Bögelein *et al.*, 2019). Apparently, the vertical mixing of assimilates should have less impact on f_{post} for Värriö compared with Hyytiälä, on account of a sparser canopy density and therewith lower intracanopy light gradients and assimilate $\delta^{13}C$

Table 1 Pearson correlations between environmental variables and annual intrinsic water-use efficiency (iWUE) of Scots pine.

Site	Variables	c_a	RH	SM	T	VPD
Hyytiälä	iWUE$_{gas}$	**0.59***	−0.19 ns	0.11 ns	0.19 ns	0.25 ns
Hyytiälä	iWUE$_{iso}$	0.53*	−0.62**	−0.50*	0.66**	**0.75*****
Hyytiälä	iWUE$_{EC}$	−0.10 ns	−0.76***	−0.54*	0.71***	**0.84*****
Värriö	iWUE$_{gas}$	**0.69****	0 ns	−0.04 ns	−0.25 ns	0 ns
Värriö	iWUE$_{iso}$	0.55*	−0.50*	−0.52 ns	0.33 ns	**0.58***
Värriö	iWUE$_{EC}$	0.45 ns	−0.88**	−0.76*	0.86**	**0.95*****

Intrinsic water-use efficiency was derived from gas exchange (iWUE$_{gas}$), tree-ring $\delta^{13}C$ (iWUE$_{iso}$), and eddy covariance (iWUE$_{EC}$) data. *, $P < 0.05$; **, $P < 0.01$; ***, $P < 0.001$; ns, not significant. The best correlation for each category is in bold. c_a, ambient CO_2 concentration; RH, relative humidity; SM, soil moisture; T, temperature; VPD, vapor pressure deficit.

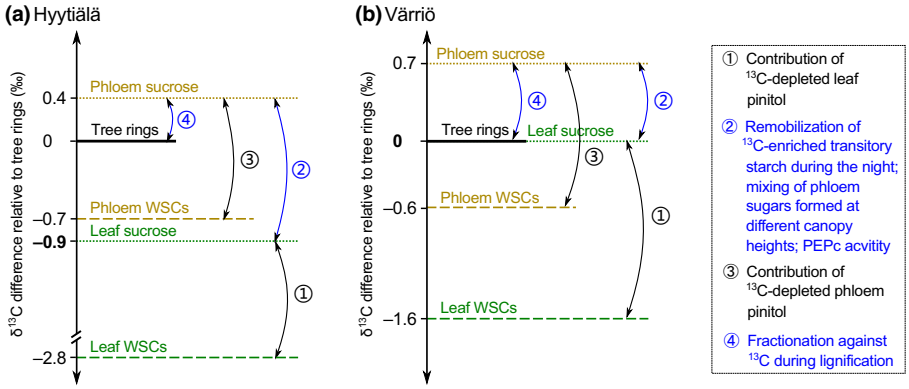

Fig. 5 $\delta^{13}C$ difference between resin-extracted tree rings and sugar pools of Scots pine in (a) Hyytiälä and (b) Värriö, together with possible underlying mechanisms. PEPc, phospho*enol*pyruvate carboxylase; WSCs, water-soluble carbohydrates.

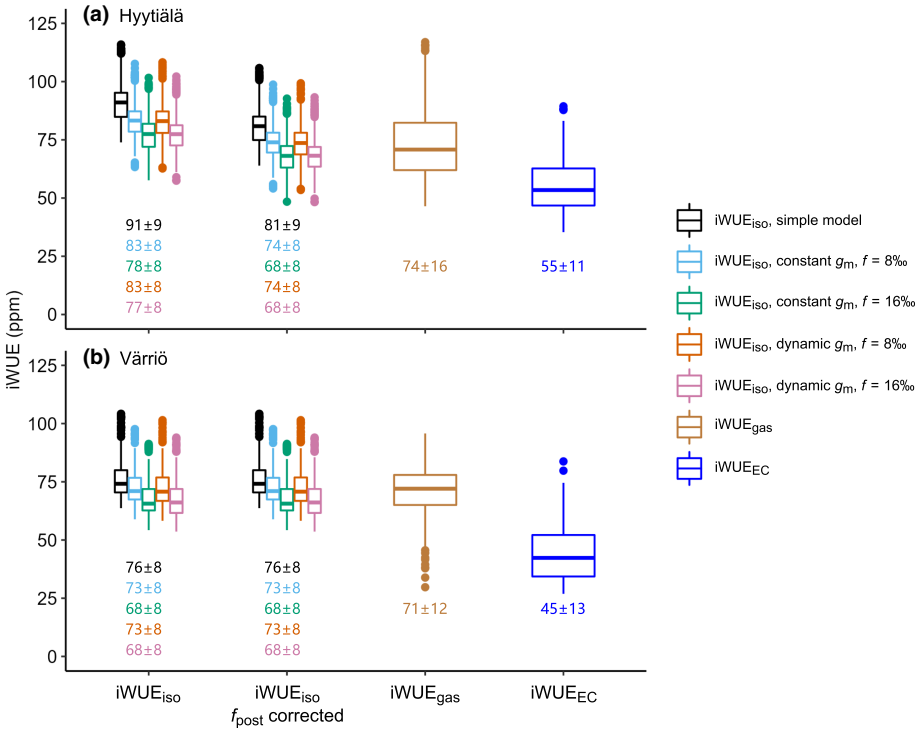

Fig. 6 Boxplot showing the intrinsic water-use efficiency (iWUE) of Scots pine in (a) Hyytiälä and (b) Värriö. $iWUE_{iso}$, $iWUE_{gas}$, and $iWUE_{EC}$ were derived from tree-ring $\delta^{13}C$, gas exchange, and eddy covariance data, respectively. $iWUE_{iso}$ was estimated from different assumptions of mesophyll conductance (g_m) and photorespiration fractionation factor (f) and corrected by postphotosynthetic $\delta^{13}C$ alteration (f_{post}). Horizontal line represents the median, box represents the interquartile range, the tails extend to 1.5 times of the interquartile range, and dots represent outliers that are outside 1.5 times of the interquartile range. Mean ± SD value (ppm) for each category is given at the bottom.

gradients in Värriö (Fig. S1). Third, f_{post} is partly determined by the activity of phospho*enol*pyruvatecarboxylase (PEPc), which favors ^{13}C when catalyzing CO_2 refixation in stems (Farquhar, 1983) and thus enriches the organic matter. Since PEPc activity varies with temperature (Chinthapalli, 2003), which differed remarkably between our study sites (Table S1), f_{post} may have differed between the two sites. Fourth, f_{post} may be affected by the ratio between ^{13}C-enriched cellulose and ^{13}C-depleted lignin (Loader *et al.*, 2003), which may vary between the two sites with different environmental conditions (Kilpelainen *et al.*, 2005).

While the explicit consideration of g_m and f generally reduced $iWUE_{iso}$ values by up to 14% (Fig. 6), it did not change the intraseasonal (Fig. S8) or interannual trends of $iWUE_{iso}$. This is in contrast to earlier studies that have reported the potential of g_m and f for modulating isotopic discrimination in long term (Keeling *et al.*, 2017; Lavergne *et al.*, 2022). Our results thereby indicate that the simplified model for $iWUE_{iso}$ is able to capture the intraseasonal trends of $iWUE_{iso}$ for our study species, albeit the accuracy of absolute values of $iWUE_{iso}$ may benefit from a better understanding of g_m dynamics in future studies. However, our results are in contrast to the report of Gimeno *et al.* (2021) for *Eucalyptus*, where a better fit between $iWUE_{gas}$ and $iWUE_{iso}$ was obtained after incorporating g_m into the calculations of $iWUE_{iso}$. This contradiction probably comes from the use of a constant g_m value or temperature-dependent g_m in this study, considering that g_m can vary with photosynthetic rate and water stress (Schiestl-Aalto *et al.*, 2021).

Environmental and physiological controls on iWUE

Differences in intraseasonal patterns of $iWUE_{iso}$, $iWUE_{EC}$, and $iWUE_{gas}$ existed in some cases, likely associated with environmental control. For instance, the intraseasonal pattern of

Table 2 Method comparison between intrinsic water-use efficiency (iWUE) derived from gas exchange ($iWUE_{gas}$), tree-ring $\delta^{13}C$ ($iWUE_{iso}$) and eddy covariance data ($iWUE_{EC}$).

	$iWUE_{gas}$	$iWUE_{iso}$	$iWUE_{EC}$
Factors affecting iWUE estimates	(1) Possible chamber artifacts, for example, occasional mechanical flaws and inconsistence in measurement systems over years (2) Uncertainties arising from limited sampling coverage	(1) Uncertainties arising from the photosynthetic discrimination model due to, for example, limited knowledge of mesophyll conductance (2) $\delta^{13}C$ alteration from leaf assimilates to tree rings, due to vertical mixing of assimilates, postphotosynthetic isotopic fractionation, and possible use of reserves	(1) Energy balance nonclosure (2) Uncertainties in net ecosystem CO_2 exchange (NEE) partitioning (3) Within-canopy gradient impacted by stand structure (4) Contribution of nontranspiratory water fluxes (5) Other sources of uncertainties, for example, aerodynamic conductance
Strength of the method	(1) High temporal resolution data, for example, at daily or diurnal scale (2) Information on species-specific dynamics	(1) Signal is archived in tree materials and can be retrieved for sites (periods) where (when) no instrumental data are available years after tree-ring formation (2) Suitable for long-term iWUE reconstructions (3) No need for on-site $\delta^{13}C$ measurements (4) Information on species-specific dynamics	(1) High temporal resolution data (2) Continuous and long-term EC records are available for many sites globally
Weakness of the method	(1) Labor-intensive and requires accessing leaves of tall trees (2) Restricted in their spatial and temporal coverage (3) Low consistency in chamber systems in long term (4) Chamber systems are prone to mechanical flaws	(1) May be influenced by other sources of isotopic discrimination	(1) Can not resolve species-specific leaf- or tree-scale dynamics (2) Subject to noise and errors in, for instance, unclosed energy balance problem and NEE partition

$iWUE_{iso}$ did not align with that of $iWUE_{gas}$ and $iWUE_{EC}$ for year 2019 in Hyytiälä (Fig. 2), possibly due to a dampened low-frequency trend in tree-ring $\delta^{13}C$ data governed by low variability in T this year. It demonstrates that a certain degree of variability in environment conditions and tree-ring $\delta^{13}C$ data within a growing season is crucial for reliable estimation of intraseasonal $iWUE_{iso}$. Furthermore, the intraseasonal pattern of $iWUE_{EC}$ is impacted by water stress. For example, for years with higher VPD in Hyytiälä (Fig. 2) and for the dry year 2012 in Värriö (Fig. 3), $iWUE_{EC}$ aligned less well with $iWUE_{iso}$ than $iWUE_{gas}$ did. This is probably because $iWUE_{EC}$ integrates the species-specific physiological response to water stress (Yi *et al.*, 2019) across various plant species over the stand (Table S1). Moreover, high spring temperatures tend to cause high uncertainties in gas exchange measurements, as the measuring shoot may recover faster than the whole canopy, resulting in divergent variability in $iWUE_{gas}$ for years 2003, 2004, 2013, and 2018 in Hyytiälä (Fig. 2).

Environmental drivers for annual iWUE were diverse across leaf ($iWUE_{gas}$), tree ($iWUE_{iso}$), and ecosystem ($iWUE_{EC}$) scales (Table 1). At leaf level, rising c_a tightly regulates $iWUE_{gas}$ (Table 1) by enhancing assimilation rate (Streit *et al.*, 2014) and reducing g_s (Brodribb *et al.*, 2009). However, the c_a effect on whole-tree level $iWUE_{iso}$ was reduced (Table 1), because the prevalent photosynthesis at lower canopy is limited by RuBP-regeneration and less sensitive to rising c_a compared with Rubisco-limited photosynthesis at top canopy (Yang *et al.*, 2020). At ecosystem level, the c_a effect was further dampened ($iWUE_{EC}$ in Table 1) due to species-specific responses of iWUE to c_a (Marchand *et al.*, 2020) and changes in leaf area and soil water savings (Lavergne *et al.*, 2019). Instead of c_a, VPD dominated changes in annual $iWUE_{iso}$ and $iWUE_{EC}$ (Table 1), as also identified in Kannenberg *et al.* (2021) and Zhang *et al.* (2019), respectively. This is probably because carbon uptake decreases less than g_s with increasing VPD (Zhang *et al.*, 2019). We also note that environmental control on iWUE varies between interannual and intraseasonal scales and from year to year, possibly related to changes in leaf area (Launiainen *et al.*, 2016) and soil moisture (Beer *et al.*, 2009).

The strengths and weaknesses of the three iWUE estimation methods

Each of the three iWUE estimation approaches has its own strengths and weaknesses (Table 2). Eddy covariance measurements have the merits in the manner that global networks, such as FLUXNET (Baldocchi *et al.*, 2001), provide EC data at varying temporal coverage up to decades (Medlyn *et al.*, 2017). However, as an ecosystem-level integrated signal, EC data are not able to discern species-specific iWUE responses (Yi *et al.*, 2019). Meanwhile, $iWUE_{EC}$ estimates have multiple sources of uncertainties (Knauer *et al.*, 2018), including within-canopy gradients, nontranspiratory water fluxes, energy balance nonclosure, issues in NEE partitioning, aerodynamic conductance, and meteorological differences between measurement height and canopy surface. Some of these uncertainties are site-specific and may vary with time. For example, within-canopy gradient, which may result in lower $iWUE_{EC}$ with a higher contribution of fluxes from the

understory (Domingues *et al.*, 2007; Sellin *et al.*, 2010), has a site-specific impact. $iWUE_{EC}$ calculated from subcanopy flux data was 30.5% lower than the gradient-integrated $iWUE_{EC}$ in Hyytiälä, whereas the difference was negligible in Värriö (6%). This site-specific trait rises from an open stand structure in Värriö (Fig. S1), which results in lower intracanopy light gradients and a higher coupling of air exchange to the atmosphere relative to a closed canopy structure in Hyytiälä (Wieser *et al.*, 2018). Moreover, $iWUE_{EC}$ is underestimated due to the contribution of nontranspiratory water fluxes (Eqn 2), mainly soil evaporation in this study as canopy evaporation should be minimal after excluding the time periods following precipitation. This underestimation is in the order of 15%, assuming soil evaporation accounted for half of forest floor ET, which contributed to *c.* 30% of total ecosystem ET at our sites (estimated from subcanopy EC data and Launiainen *et al.*, 2005). However, this proportion would change with the increase in leaf area index in Hyytiälä (Table S1) but stay almost constant over the years with roughly unchanged leaf area index in Värriö.

Leaf gas exchange measurements have the advantages of tracing instantaneous changes in iWUE, but this method is labor-intensive and requires accessing leaves of tall trees (Yi *et al.*, 2019). Meanwhile, even though a global compilation of gas exchange measurements is available (Lin *et al.*, 2015), there is currently a lack of long-term continuous datasets. Also, $iWUE_{gas}$ estimates are subject to uncertainties regarding chamber artifacts, limited sampling coverage, and low consistency in measurement systems in long term. Occasional mechanical flaws, for example leaks, and possible damages to the measuring shoots may affect the observed seasonal cycle. Limited sampling coverage on one or several measuring shoots on the top canopy may induce uncertainties, for example, during warm springs. Changes in measurement systems over years may bias the interannual trend of $iWUE_{gas}$. Nevertheless, not including boundary layer conductance in calculating $iWUE_{gas}$ overall has a limited impact on absolute values (Seibt *et al.*, 2008) and intraseasonal patterns of $iWUE_{gas}$ (Figs 2, 3).

Tree-ring $\delta^{13}C$ can be retrieved even decades or centuries after tree-ring formation without laborious work on site (Cernusak, 2020). Hence, a major advantage of tree-ring $\delta^{13}C$ records is their potential for reconstructing long-term $iWUE_{iso}$. Accuracy of $iWUE_{iso}$ estimates can be further improved by a better understanding of f_{post}, g_m, and f. More importantly, our study shows that iWUE can be obtained from tree-ring $\delta^{13}C$ at intraseasonal scale with reasonable effort using LA-IRMS, extending the application of this iWUE estimation method from annual resolution to intraseasonal resolution. This finding is inspiring in the way that it provides a valuable method for intraseasonal iWUE estimates, especially for sites and periods where and when no gas exchange or EC data are available.

Conclusions

This work presented the first comparison between intraseasonal and interannual iWUE signal derived from leaf gas exchange, tree-ring $\delta^{13}C$, and EC data, resting on a unique set of 18-yr-long records in two boreal forest sites. The alignment in intraseasonal iWUE trends across different methods demonstrated the reliability of tree-ring $\delta^{13}C$ derived intraseasonal iWUE estimates. This result is of special significance to studies, which seek to detect intraseasonal tree physiological dynamics in terms of iWUE but with no access to instrumental data. The absolute values of iWUE across different datasets can be reconciled by taking into account an overestimation in $iWUE_{iso}$ of up to 11% due to f_{post}, and of up to 14% due to nonexplicit consideration of mesophyll and photorespiratory effects. A significant increasing interannual trend existed in $iWUE_{gas}$, but not in $iWUE_{iso}$ or $iWUE_{EC}$, for both sites, possibly resulting from a predominant control of c_a on $iWUE_{gas}$ but VPD control on $iWUE_{iso}$ and $iWUE_{EC}$. We encourage more across-method comparisons of iWUE at various temporal and spatial scales in the future. Such studies will not only deepen our understanding of how trees physiologically adapt to climate change but also provide insights into ecological models in respect of linking ecological information across scales.

Acknowledgements

We would like to thank Esko Karvinen, Aino Ovaska, Salla Kuittinen, Jukka Kärki, Aino Seppänen, Marine Manche, Fana Teferra, Ari Kinnunen, Janne Levula, Juho Aalto, Teuvo Hietajärvi, Tarmo Kylli, Bartosz Adamczyk, Petri Kilpeläinen, and Haoran Li for their help in field work. Further thanks go to Manuela Oettli for HPLC-IRMS $\delta^{13}C$ analysis, Antti Tiisanoja, Natalia Kiuru, and Nikol Ilchevska for microcore preparation and microscopy analysis. This study was financially supported by the European Research Council (no. 755865), the Academy of Finland (nos. 295319, 323843), the Finnish Cultural Foundation (no. 00221014), and the Swiss National Science Foundation SNSF (no. 207360).

Competing interests

None declared.

Author contributions

KTR-G and YT planned and designed the study. YT, PS-A, KTR-G, ES and GY conducted fieldwork. YT prepared sugar samples for $\delta^{13}C$ analysis. GY prepared tree-ring samples for $\delta^{13}C$ analysis. ES conducted bulk and LA-IRMS $\delta^{13}C$ analysis. MS conducted HPLC-IRMS $\delta^{13}C$ analysis. PK calculated eddy covariance and leaf gas exchange data. PS-A modeled tree-ring growth via CASSIA. YT and TJ conducted xylogenesis observations. YT conducted data analysis. YT was responsible for writing the manuscript. JB and all other authors contributed to the interpretation of data and the writing of the manuscript at various stages.

ORCID

Jaana Bäck https://orcid.org/0000-0002-6107-667X
Tuula Jyske https://orcid.org/0000-0002-0459-4358
Pasi Kolari https://orcid.org/0000-0001-7271-633X

Katja T. Rinne-Garmston https://orcid.org/0000-0001-9793-2549
Elina Sahlstedt https://orcid.org/0000-0001-8612-6007
Matthias Saurer https://orcid.org/0000-0002-3954-3534
Pauliina Schiestl-Aalto https://orcid.org/0000-0003-1369-1923
Yu Tang https://orcid.org/0000-0002-2851-4762
Giles Young https://orcid.org/0000-0002-1102-3553

Data availability

The data that support the findings of this study are openly available in Figshare at doi: 10.6084/m9.figshare.21267963.v1.

References

Aalto J, Kolari P, Hari P, Kerminen V-M, Schiestl-Aalto P, Aaltonen H, Levula J, Siivola E, Kulmala M, Bäck J. 2014. New foliage growth is a significant, unaccounted source for volatiles in boreal evergreen forests. *Biogeosciences* **11**: 1331–1344.

Altimir N, Kolari P, Tuovinen J, Vesala T, Bäck J, Suni T, Kulmala M, Hari P. 2006. Foliage surface ozone deposition: a role for surface moisture? *Biogeosciences* **3**: 209–228.

Altimir N, Vesala T, Keronen P, Kulmala M, Hari P. 2002. Methodology for direct field measurements of ozone flux to foliage with shoot chambers. *Atmospheric Environment* **36**: 19–29.

Aubinet M, Vesala T, Papale D. 2012. *Eddy covariance: a practical guide to measurement and data analysis.* Dordrecht, the Netherlands: Springer.

Baldocchi D, Falge E, Fuentes J, Goldstein A, Katul G, Law B, Lee X, Malhi Y, Meyers T, Munger W *et al.* 2001. FLUXNET: a new tool to study the temporal and spatial variability of ecosystem-scale carbon dioxide, water vapor, and energy flux densities. *Bulletin of the American Meteorological Society* **82**: 2415–2434.

Beer C, Ciais P, Reichstein M, Baldocchi D, Law BE, Papale D, Soussana J-F, Ammann C, Buchmann N, Frank D *et al.* 2009. Temporal and among-site variability of inherent water use efficiency at the ecosystem level. *Global Biogeochemical Cycles* **23**: GB2018.

Belmecheri S, Lavergne A. 2020. Compiled records of atmospheric CO_2 concentrations and stable carbon isotopes to reconstruct climate and derive plant ecophysiological indices from tree rings. *Dendrochronologia* **63**: 125748.

Bernacchi CJ, Singsaas EL, Pimentel C, Portis AR Jr, Long SP. 2001. Improved temperature response functions for models of Rubisco-limited photosynthesis. *Plant, Cell & Environment* **24**: 253–259.

Bögelein R, Lehmann MM, Thomas FM. 2019. Differences in carbon isotope leaf-to-phloem fractionation and mixing patterns along a vertical gradient in mature European beech and Douglas fir. *New Phytologist* **222**: 1803–1815.

Brodribb TJ, McAdam SAM, Jordan GJ, Feild TS. 2009. Evolution of stomatal responsiveness to CO_2 and optimization of water-use efficiency among land plants. *New Phytologist* **183**: 839–847.

Busch FA, Holloway-Phillips M, Stuart-Williams H, Farquhar GD. 2020. Revisiting carbon isotope discrimination in C_3 plants shows respiration rules when photosynthesis is low. *Nature Plants* **6**: 245–258.

Cernusak LA. 2020. Gas exchange and water-use efficiency in plant canopies. *Plant Biology* **22**: 52–67.

Chinthapalli B. 2003. Dramatic difference in the responses of phosphoenolpyruvate carboxylase to temperature in leaves of C_3 and C_4 plants. *Journal of Experimental Botany* **54**: 707–714.

Domingues TF, Martinelli LA, Ehleringer JR. 2007. Ecophysiological traits of plant functional groups in forest and pasture ecosystems from eastern Amazônia, Brazil. *Plant Ecology* **193**: 101–112.

Evans JR, von Caemmerer S. 2013. Temperature responses of mesophyll conductance differ greatly between species. *Plant, Cell & Environment* **36**: 745–756.

Farquhar GD. 1983. On the nature of carbon isotope discrimination in C_4 species. *Functional Plant Biology* **10**: 205–226.

Farquhar GD, Ehleringer IJR, Hubick KT. 1989. Carbon isotope discrimination and photosynthesis. *Annual Review of Plant Biology* **40**: 503–537.

Farquhar GD, O'Leary MH, Berry JA. 1982. On the relationship between carbon isotope discrimination and the intercellular carbon dioxide concentration in leaves. *Functional Plant Biology* **9**: 121–127.

Fiorella RP, Kannenberg SA, Anderegg WRL, Monson RK, Ehleringer JR. 2022. Heterogeneous isotope effects decouple conifer leaf and branch sugar $\delta^{18}O$ and $\delta^{13}C$. *Oecologia* **198**: 357–370.

Fonti M, Vaganov E, Wirth C, Shashkin A, Astrakhantseva N, Schulze ED. 2018. Age-effect on intra-annual $\delta^{13}C$-variability within Scots pine tree-rings from central Siberia. *Forests* **9**: 364.

Frank DC, Poulter B, Saurer M, Esper J, Huntingford C, Helle G, Treydte K, Zimmermann NE, Schleser GH, Ahlström A *et al.* 2015. Water-use efficiency and transpiration across European forests during the Anthropocene. *Nature Climate Change* **5**: 579–583.

Gessler A, Brandes E, Buchmann N, Helle G, Rennenberg H, Barnard RL. 2009. Tracing carbon and oxygen isotope signals from newly assimilated sugars in the leaves to the tree-ring archive. *Plant, Cell & Environment* **32**: 780–795.

Gessler A, Ferrio JP. 2022. Chapter 13: postphotosynthetic fractionation in leaves, phloem and stem. In: Siegwolf RTW, Brooks JR, Roden J, Saurer M, eds. *Stable isotopes in tree rings.* Cham, Switzerland: Springer, 381–396.

Ghashghaie J, Badeck F-W, Lanigan G, Nogués S, Tcherkez G, Deléens E, Cornic G, Griffiths H. 2003. Carbon isotope fractionation during dark respiration and photorespiration in C_3 plants. *Phytochemistry Reviews* **2**: 145–161.

Gimeno TE, Campany CE, Drake JE, Barton CVM, Tjoelker MG, Ubierna N, Marshall JD. 2021. Whole-tree mesophyll conductance reconciles isotopic and gas-exchange estimates of water-use efficiency. *New Phytologist* **229**: 2535–2547.

Guerrieri R, Belmecheri S, Ollinger SV, Asbjornsen H, Jennings K, Xiao J, Stocker BD, Martin M, Hollinger DY, Bracho-Garrillo R *et al.* 2019. Disentangling the role of photosynthesis and stomatal conductance on rising forest water-use efficiency. *Proceedings of the National Academy of Sciences, USA* **116**: 16909–16914.

Kannenberg SA, Driscoll AW, Szejner P, Anderegg WRL, Ehleringer JR. 2021. Rapid increases in shrubland and forest intrinsic water-use efficiency during an ongoing megadrought. *Proceedings of the National Academy of Sciences, USA* **118**: e2118052118.

Keeling RF, Graven HD, Welp LR, Resplandy L, Bi J, Piper SC, Sun Y, Bollenbacher A, Meijer HAJ. 2017. Atmospheric evidence for a global secular increase in carbon isotopic discrimination of land photosynthesis. *Proceedings of the National Academy of Sciences, USA* **114**: 10361–10366.

Keenan TF, Hollinger DY, Bohrer G, Dragoni D, Munger JW, Schmid HP, Richardson AD. 2013. Increase in forest water-use efficiency as atmospheric carbon dioxide concentrations rise. *Nature* **499**: 324–327.

Keenan TF, Migliavacca M, Papale D, Baldocchi D, Reichstein M, Torn M, Wutzler T. 2019. Widespread inhibition of daytime ecosystem respiration. *Nature Ecology & Evolution* **3**: 407–415.

Kilpelainen A, Peltola H, Ryyppo A, Kellomaki S. 2005. Scots pine responses to elevated temperature and carbon dioxide concentration: growth and wood properties. *Tree Physiology* **25**: 75–83.

Knauer J, Zaehle S, Medlyn BE, Reichstein M, Williams CA, Migliavacca M, De Kauwe MG, Werner C, Keitel C, Kolari P *et al.* 2018. Towards physiologically meaningful water-use efficiency estimates from eddy covariance data. *Global Change Biology* **24**: 694–710.

Kolari P, Bäck J, Taipale R, Ruuskanen TM, Kajos MK, Rinne J, Kulmala M, Hari P. 2012. Evaluation of accuracy in measurements of VOC emissions with dynamic chamber system. *Atmospheric Environment* **62**: 344–351.

Kolari P, Kulmala L, Pumpanen J, Launiainen S, Ilvesniemi H, Hari P, Nikinmaa E. 2009. CO_2 exchange and component CO_2 fluxes of a boreal Scots pine forest. *Boreal Environment Research* **14**: 23.

Kress A, Saurer M, Siegwolf RTW, Frank DC, Esper J, Bugmann H. 2010. A 350 year drought reconstruction from alpine tree ring stable isotopes. *Global Biogeochemical Cycles* **24**: GB2011.

Kulmala L, Pumpanen J, Kolari P, Dengel S, Berninger F, Köster K, Matkala L, Vanhatalo A, Vesala T, Bäck J. 2019. Inter- and intra-annual dynamics of photosynthesis differ between forest floor vegetation and tree canopy in a subarctic Scots pine stand. *Agricultural and Forest Meteorology* **271**: 1–11.

Launiainen S, Katul GG, Kolari P, Lindroth A, Lohila A, Aurela M, Varlagin A, Grelle A, Vesala T. 2016. Do the energy fluxes and surface conductance of boreal coniferous forests in Europe scale with leaf area? *Global Change Biology* **22**: 4096–4113.

Launiainen S, Katul GG, Leppä K, Kolari P, Aslan T, Grönholm T, Korhonen L, Mammarella I, Vesala T. 2022. Does growing atmospheric CO_2 explain increasing carbon sink in a boreal coniferous forest? *Global Change Biology* **28**: 2910–2929.

Launiainen S, Rinne J, Pumpanen J, Kulmala L, Kolari P, Keronen P, Siivola E, Pohja T, Hari P, Vesala T. 2005. Eddy covariance measurements of CO_2 and sensible and latent heat fluxes during a full year in a boreal pine forest trunk-space. *Boreal Environment Research* **10**: 569–588.

Lavergne A, Graven H, De Kauwe MG, Keenan TF, Medlyn BE, Prentice IC. 2019. Observed and modelled historical trends in the water-use efficiency of plants and ecosystems. *Global Change Biology* **25**: 2242–2257.

Lavergne A, Hemming D, Prentice IC, Guerrieri R, Oliver RJ, Graven H. 2022. Global decadal variability of plant carbon isotope discrimination and its link to gross primary production. *Global Change Biology* **28**: 524–541.

Leavitt SW, Long A. 1984. Sampling strategy for stable carbon isotope analysis of tree rings in pine. *Nature* **311**: 145–147.

Lin Y-S, Medlyn BE, Duursma RA, Prentice IC, Wang H, Baig S, Eamus D, de Dios VR, Mitchell P, Ellsworth DS *et al.* 2015. Optimal stomatal behaviour around the world. *Nature Climate Change* **5**: 459–464.

Liu X, Wang W, Xu G, Zeng X, Wu G, Zhang X, Qin D. 2014. Tree growth and intrinsic water-use efficiency of inland riparian forests in northwestern China: evaluation via ^{13}C and ^{18}O analysis of tree rings. *Tree Physiology* **34**: 966–980.

Loader NJ, McCarroll D, Barker S, Jalkanen R, Grudd H. 2017. Inter-annual carbon isotope analysis of tree-rings by laser ablation. *Chemical Geology* **466**: 323–326.

Loader NJ, Robertson I, Barker AC, Switsur VR, Waterhouse J. 1997. An improved technique for the batch processing of small wholewood samples to α-cellulose. *Chemical Geology* **136**: 313–317.

Loader NJ, Robertson I, McCarroll D. 2003. Comparison of stable carbon isotope ratios in the whole wood, cellulose and lignin of oak tree-rings. *Palaeogeography, Palaeoclimatology, Palaeoecology* **196**: 395–407.

Ma WT, Tcherkez G, Wang XM, Schäufele R, Schnyder H, Yang Y, Gong XY. 2021. Accounting for mesophyll conductance substantially improves ^{13}C-based estimates of intrinsic water-use efficiency. *New Phytologist* **229**: 1326–1338.

Mammarella I, Peltola O, Nordbo A, Järvi L, Rannik Ü. 2016. Quantifying the uncertainty of eddy covariance fluxes due to the use of different software packages and combinations of processing steps in two contrasting ecosystems. *Atmospheric Measurement Techniques* **9**: 4915–4933.

Marchand W, Girardin MP, Hartmann H, Depardieu C, Isabel N, Gauthier S, Boucher É, Bergeron Y. 2020. Strong overestimation of water-use efficiency responses to rising CO_2 in tree-ring studies. *Global Change Biology* **26**: 4538–4558.

Markkanen T, Rannik Ü, Keronen P, Suni T, Vesala T. 2001. Eddy covariance fluxes over a boreal Scots pine forest. *Boreal Environment Research* **6**: 65–78.

Martínez-Sancho E, Dorado-Liñán I, Gutiérrez Merino E, Matiu M, Helle G, Heinrich I, Menzel A. 2018. Increased water-use efficiency translates into contrasting growth patterns of Scots pine and sessile oak at their southern distribution limits. *Global Change Biology* **24**: 1012–1028.

Mathias JM, Thomas RB. 2021. Global tree intrinsic water use efficiency is enhanced by increased atmospheric CO_2 and modulated by climate and plant functional types. *Proceedings of the National Academy of Sciences, USA* **118**: e2014286118.

McCarroll D, Loader NJ. 2004. Stable isotopes in tree rings. *Quaternary Science Reviews* **23**: 771–801.

McCarroll D, Whitney M, Young GHF, Loader NJ, Gagen MH. 2017. A simple stable carbon isotope method for investigating changes in the use of recent versus old carbon in oak. *Tree Physiology* **37**: 1021–1027.

McLeod A. 2011. *Kendall: Kendall rank correlation and Mann-Kendall trend test, v.2.2.1.* [WWW document] URL https://CRAN.R-project.org/package=Kendall [accessed 28 April 2022].

Medlyn BE, De Kauwe MG, Lin Y, Knauer J, Duursma RA, Williams CA, Arneth A, Clement R, Isaac P, Limousin J *et al.* 2017. How do leaf and ecosystem measures of water-use efficiency compare? *New Phytologist* **216**: 758–770.

Mencuccini M, Hölttä T. 2010. The significance of phloem transport for the speed with which canopy photosynthesis and belowground respiration are linked. *New Phytologist* **185**: 189–203.

Michelot A, Eglin T, Dufrêne E, Lelarge-Trouverie C, Damesin C. 2011. Comparison of seasonal variations in water-use efficiency calculated from the carbon isotope composition of tree rings and flux data in a temperate forest. *Plant, Cell & Environment* **34**: 230–244.

Osmond CB, Björkman O, Anderson DJ. 1980. Chapter 9: photosynthesis. In: Durham WDB, Athens FG, Würzburg OLL, Oak Ridge JSO, eds. *Physiological processes in plant ecology: toward a synthesis with atriplex*. Berlin, Germany: Springer-Verlag, 291–377.

R Core Team. 2020. *R: a language and environment for statistical computing, v.4.0.0.* Vienna, Austria: R Foundation for Statistical Computing. [WWW document] URL http://www.r-project.org [accessed 15 May 2020].

Rinne KT, Saurer M, Kirdyanov AV, Loader NJ, Bryukhanova MV, Werner RA, Siegwolf RTW. 2015. The relationship between needle sugar carbon isotope ratios and tree rings of larch in Siberia. *Tree Physiology* **35**: 1192–1205.

Rinne KT, Saurer M, Streit K, Siegwolf RTW. 2012. Evaluation of a liquid chromatography method for compound-specific $\delta^{13}C$ analysis of plant carbohydrates in alkaline media. *Rapid Communications in Mass Spectrometry* **26**: 2173–2185.

Rinne-Garmston K, Helle G, Lehmann M, Sahlstedt E, Schleucher J, Waterhouse J. 2022. Chapter 7: newer developments in tree ring stable isotope methods. In: Siegwolf RTW, Brooks JR, Roden J, Saurer M, eds. *Stable isotopes in tree rings*. Cham, Switzerland: Springer, 215–249.

Schiestl-Aalto P, Kulmala L, Mäkinen H, Nikinmaa E, Mäkelä A. 2015. CASSIA – a dynamic model for predicting intra-annual sink demand and interannual growth variation in Scots pine. *New Phytologist* **206**: 647–659.

Schiestl-Aalto P, Stangl ZR, Tarvainen L, Wallin G, Marshall J, Mäkelä A. 2021. Linking canopy-scale mesophyll conductance and phloem sugar $\delta^{13}C$ using empirical and modelling approaches. *New Phytologist* **229**: 3141–3155.

Schleser GH. 1990. Investigations of the $\delta^{13}C$ pattern in leaves of *Fagus sylvatica* L. *Journal of Experimental Botany* **41**: 565–572.

Schubert BA, Jahren AH. 2018. Incorporating the effects of photorespiration into terrestrial paleoclimate reconstruction. *Earth-Science Reviews* **177**: 637–642.

Schulze B, Wirth C, Linke P, Brand WA, Kuhlmann I, Horna V, Schulze E-D. 2004. Laser ablation-combustion-GC-IRMS – a new method for online analysis of intra-annual variation of ^{13}C in tree rings. *Tree Physiology* **24**: 1193–1201.

Seibt U, Rajabi A, Griffiths H, Berry JA. 2008. Carbon isotopes and water use efficiency: sense and sensitivity. *Oecologia* **155**: 441–454.

Sellin A, Eensalu E, Niglas A. 2010. Is distribution of hydraulic constraints within tree crowns reflected in photosynthetic water-use efficiency? An example of Betula pendula. *Ecological Research* **25**: 173–183.

Soudant A, Loader NJ, Bäck J, Levula J, Kljun N. 2016. Intra-annual variability of wood formation and $\delta^{13}C$ in tree-rings at Hyytiälä, Finland. *Agricultural and Forest Meteorology* **224**: 17–29.

Stangl ZR, Tarvainen L, Wallin G, Ubierna N, Räntfors M, Marshall JD. 2019. Diurnal variation in mesophyll conductance and its influence on modelled water-use efficiency in a mature boreal *Pinus sylvestris* stand. *Photosynthesis Research* **141**: 53–63.

Streit K, Siegwolf RTW, Hagedorn F, Schaub M, Buchmann N. 2014. Lack of photosynthetic or stomatal regulation after 9 years of elevated [CO_2] and 4 years of soil warming in two conifer species at the alpine treeline. *Plant, Cell & Environment* **37**: 315–326.

Sun Y, Gu L, Dickinson RE, Norby RJ, Pallardy SG, Hoffman FM. 2014. Impact of mesophyll diffusion on estimated global land CO_2 fertilization. *Proceedings of the National Academy of Sciences, USA* **111**: 15774–15779.

Tang Y, Schiestl-Aalto P, Lehmann MM, Saurer M, Sahlstedt E, Kolari P, Leppä K, Bäck J, Rinne-Garmston K. In press. Estimating intra-seasonal photosynthetic discrimination and water use efficiency using $\delta^{13}C$ of leaf sucrose of Scots pine. *Journal of Experimental Botany*. doi: 10.1093/jxb/erac413.

Uddling J, Wallin G. 2012. Interacting effects of elevated CO_2 and weather variability on photosynthesis of mature boreal Norway spruce agree with biochemical model predictions. *Tree Physiology* **32**: 1509–1521.

Vesala T, Suni T, Rannik Ü, Keronen P, Markkanen T, Sevanto S, Grönholm T, Smolander S, Kulmala M, Ilvesniemi H *et al.* 2005. Effect of thinning on surface fluxes in a boreal forest: thinning and surface fluxes in boreal forest. *Global Biogeochemical Cycles* **19**: GB2001.

Vincent-Barbaroux C, Berveiller D, Lelarge-Trouverie C, Maia R, Máguas C, Pereira J, Chaves MM, Damesin C. 2019. Carbon-use strategies in stem radial growth of two oak species, one temperate deciduous and one mediterranean evergreen: what can be inferred from seasonal variations in the $\delta^{13}C$ of the current year ring? *Tree Physiology* **39**: 1329–1341.

Wanek W, Heintel S, Richter A. 2001. Preparation of starch and other carbon fractions from higher plant leaves for stable carbon isotope analysis. *Rapid Communications in Mass Spectrometry* **15**: 1136–1140.

Waterhouse JS, Switsur VR, Barker AC, Carter AHC, Hemming DL, Loader NJ, Robertson I. 2004. Northern European trees show a progressively diminishing response to increasing atmospheric carbon dioxide concentrations. *Quaternary Science Reviews* **23**: 803–810.

Werner RA, Brand WA. 2001. Referencing strategies and techniques in stable isotope ratio analysis. *Rapid Communications in Mass Spectrometry* **15**: 501–519.

Wieser G, Oberhuber W, Waldboth B, Gruber A, Matyssek R, Siegwolf RTW, Grams TEE. 2018. Long-term trends in leaf level gas exchange mirror tree-ring derived intrinsic water-use efficiency of *Pinus cembra* at treeline during the last century. *Agricultural and Forest Meteorology* **248**: 251–258.

Yang J, Medlyn BE, De Kauwe MG, Duursma RA, Jiang M, Kumarathunge D, Crous KY, Gimeno TE, Wujeska-Klause A, Ellsworth DS. 2020. Low sensitivity of gross primary production to elevated CO_2 in a mature eucalypt woodland. *Biogeosciences* **17**: 265–279.

Yi K, Maxwell JT, Wenzel MK, Roman DT, Sauer PE, Phillips RP, Novick KA. 2019. Linking variation in intrinsic water-use efficiency to isohydricity: a comparison at multiple spatiotemporal scales. *New Phytologist* **221**: 195–208.

Zhang Q, Ficklin DL, Manzoni S, Wang L, Way D, Phillips RP, Novick KA. 2019. Response of ecosystem intrinsic water use efficiency and gross primary productivity to rising vapor pressure deficit. *Environmental Research Letters* **14**: 074023.

Supporting Information

Additional Supporting Information may be found online in the Supporting Information section at the end of the article.

Fig. S1 Locations and photographs of the study sites in Finland.

Fig. S2 Intraseasonal tree-ring $\delta^{13}C$ of Scots pine from 2002 to 2019 in Hyytiälä.

Fig. S3 Intraseasonal tree-ring $\delta^{13}C$ of Scots pine from 2002 to 2019 in Värriö.

Fig. S4 Comparison of growth curves of Scots pine from CASSIA model and from xylogenesis observations.

Fig. S5 Relationship between event-based $\delta^{13}C$ of atmospheric CO_2 ($\delta^{13}C_{air}$) and concentration of ambient CO_2 (c_a) in Pallas.

Fig. S6 Comparison of $\delta^{13}C$ signal in leaf sugars, phloem sugars, and resin-extracted wood of Scots pine in Hyytiälä and Värriö in 2018.

Fig. S7 Boxplot showing the intrinsic water-use efficiency of Scots pine averaged for the growing periods of earlywood, latewood, and whole ring.

Fig. S8 Boxplot showing correlations between intraseasonal intrinsic water-use efficiency of Scots pine derived from different methods under different mesophyll and photorespiratory assumptions.

Fig. S9 Across-border correlations in tree-ring $\delta^{13}C$ of Scots pine, which denotes the degree of use of previous-year reserves.

Methods S1 LA-IRMS systems.

Methods S2 Tracheid growth curves from xylogenesis observations and CASSIA model.

Methods S3 Dynamic g_m assumption.

Table S1 General description, site characteristics, and data availability for our study sites.

Please note: Wiley is not responsible for the content or functionality of any Supporting Information supplied by the authors. Any queries (other than missing material) should be directed to the *New Phytologist* Central Office.